Isotope shifts of double-excitation resonances in helium

Y. H. Jiang,[1,2,*] R. Püttner,[1] M. Martins,[1] R. Follath,[3] J. M. Rost,[2] and G. Kaindl[1]
[1]*Institut für Experimentalphysik, Freie Universität Berlin, Arnimallee 14, D-14195 Berlin-Dahlem, Germany*
[2]*Max-Planck-Institut für Physik Komplexer Systeme, Nöthnitzer Strasse 38, D-01187 Dresden, Germany*
[3]*BESSY GmbH, Albert-Einstein-Strasse 15, D-12489 Berlin, Germany*
(Received 8 January 2004; published 6 May 2004)

Isotopic effects on double-excitation resonances in ^{3}He and ^{4}He were observed in photoionization spectra using synchrotron radiation with high monochromator resolution. In ^{3}He, the resonances were found to be shifted to lower energies with respect to ^{4}He by $\Delta E = 3.06 \pm 0.07$ meV, in good agreement with theoretical expectations based on normal and specific mass shifts. From the experimental data, the resonance parameters E_r, Γ, and q of the resonances $2,-1_3$, $2,1_4$, and $2,0_7$ were analyzed in detail using a double-convolution fit procedure that considers the different Doppler broadenings of the states in ^{3}He and ^{4}He. In this way, the resolution function of the monochromator could be derived, which can be accounted for in a quantitative way on the basis of the properties of undulator radiation and the optical design of the monochromator.

DOI: 10.1103/PhysRevA.69.052703 PACS number(s): 32.80.Dz, 32.80.Rm, 07.85.Qe

I. INTRODUCTION

Ever since the pioneering work of Madden and Codling four decades ago [1], the autoionizing $^1P^o$ Rydberg resonances of ^{4}He have been studied extensively both experimentally [2–8] and theoretically [9–11]. The progress in the experimental work proceeded along with the development of synchrotron-radiation facilities and high-resolution, grazing-incidence monochromators. State-of-the-art monochromators, with an experimental resolution of less than 1 meV at photon energies of $h\nu \cong 64$ eV, allowed to investigate very narrow resonances, such as, e.g., the $2,-1_n$ series in doubly excited helium [3,4]. These precise measurements provide strong support for a description of the decay dynamics of the autoinoization process in two-electron atoms within a molecular picture [10].

Isotope shifts are well known to contain contributions from the mass shift (MS) and the volume shift (VS), where the later is caused by a difference in the nuclear charge distributions of the two isotopes under study; for light elements, the VS is negligibly small as compared to the MS. The MS consists of two contributions, the normal mass shift (NMS) and the specific mass shift (SMS). The NMS, which is the well-known Bohr-reduced mass correction, can be evaluated exactly, while the SMS, also called the polarization mass shift, originates from exchange effects and repulsion between the electrons [12]. While ^{3}He-^{4}He isotope shifts have been studied before in the energy region of the $1\ ^1S \rightarrow 2\ ^1P$ [13] and $2\ ^3S \rightarrow 2\ ^3P$ [14] optical transitions using advanced laser techniques, the present work reports on a measurement of isotope shifts in the energy region of the doubly excited states of helium.

With substantial improvements in monochromator resolution in recent years to values of $\Omega_M \leqslant 1$ meV [full width at half maximum (FWHM)] at $h\nu \cong 64$ eV [3,15,16], the total experimental widths of narrow resonances have become comparable to the Doppler broadening of resonance lines in light atoms, which amounts to $\cong 0.4$ meV (FWHM) at $h\nu \cong 64$ eV for ^{4}He at 300 K. Therefore, a reliable analysis of narrow resonance lines should take into account both the monochromator resolution and the Doppler broadening by applying a double-convolution fit procedure. In this way, we succeeded in deriving from the experimental spectra the monochromator-resolution function, which differs considerably from a pure Gaussian function that has been widely used in the analysis of spectral profiles. The derived resolution function can be explained on the basis of the properties of undulator radiation and the optical design of the employed extreme ultraviolet (XUV) monochromator. With this improved understanding of monochromator resolution, we discuss some of the points that must be considered when the highest monochromator resolution is aimed for.

In the present work, the doubly excited $^1P^o$ resonances of helium are denoted N,K_n according to the simplified classification scheme of Herrick and Sinanoğlu [17], where N and n stand for the dissociation limit of a channel and the running index of a Rydberg series, respectively. In an independent particle picture, $N(n)$ corresponds to the quantum number of the inner (outer) electron, while K represents the angular-correlation quantum number [18].

II. EXPERIMENTAL DETAILS

The experiments were performed at the Berliner Elektronenspeicherring für Synchrotronstrahlung (BESSY II) using the undulator beamline U125/1-PGM, which provides ultrahigh resolution at photon energies around 64 eV, with $\Omega_M \leqslant 1$ meV (FWHM). The photoionization spectra were taken with a gas ionization cell that was separated from the UHV of the monochromator by a 1000-Å-thick aluminum window. During the experiments, the gas cell was filled with the gas under study, in the present case with a mixture of ^{3}He and ^{4}He at a pressure of $\cong 400$ μbar. From the observed spectral intensities (see Fig. 2), the ratio of partial pressures of ^{4}He and ^{3}He in the studied gas mixture was estimated to be

*Electronic address: yhjiang@physik.fu-berlin.de

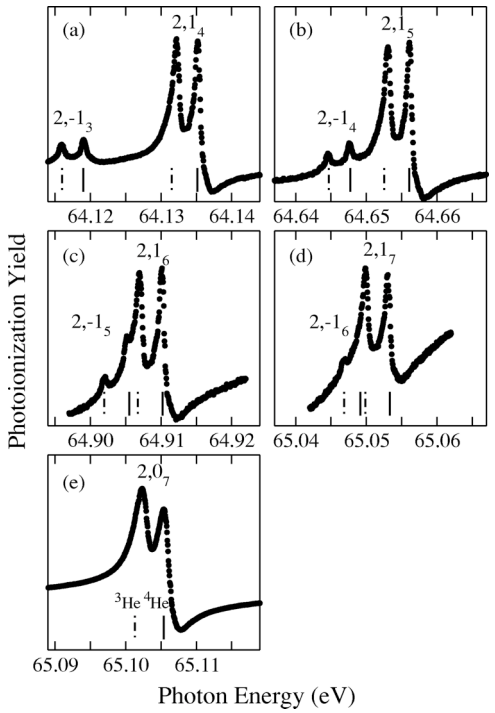

FIG. 1. Photoionization spectra of the resonances $2,-1_n$ (with $n=3$ to 6), $2,1_n$ (with $n=4$ to 7), and $2,0_7$ in ^{3}He and ^{4}He, respectively, measured on a ^{3}He-^{4}He gas mixture. The resonance positions are marked for ^{4}He (^{3}He) by solid (dash-dotted) vertical bars.

$\cong 5:4$. Due to sizeable isotope shifts in the resonance energies of ^{3}He and ^{4}He, the photoionization spectra of both isotopes could be measured simultaneously, which allows one to determine isotope shifts with high accuracy rather independent of the absolute energy calibration. The absolute photon energies given in the present work were calibrated with respect to the energy position of the $2,-1_3$ resonance as given by Domke *et al.* [4].

III. EXPERIMENTAL RESULTS AND DATA ANALYSIS

Figure 1 presents as overview of the measured spectra, with the resonances $2,-1_n$ ($n=3$ to 6), $2,1_n$ ($n=4$ to 7), and $2,0_7$ in ^{3}He and ^{4}He, respectively. Each resonance is split into two peaks due to the isotopic effects, and the corresponding energy splittings are derived as 3.06 ± 0.07 meV, in good agreement with theoretical considerations as given below. The resonance $2,-1_6$ in ^{4}He cannot be resolved due to an overlap with the resonance $2,1_7$ of ^{3}He.

The resonance lines in the spectra of Fig. 1 exhibit pronounced Fano profiles, which originate from an interference between direct photoionization and excitation into an autoionization channel. This results in Fano profiles of the form [19,20]

$$\sigma(E) = \sigma_a \frac{(q+\epsilon)^2}{1+\epsilon^2} + \sigma_b, \quad \text{with } \epsilon = 2\frac{E-E_r}{\Gamma}. \tag{1}$$

Here, E_r is the resonance energy and Γ the natural width that is determined by the decay rate of the resonance, representing the discrete-continuum mixing strength. The Fano parameter q represents the ratio of the dipole matrix element of a transition to a discrete state to that of a transition to the continuum, which interacts with the discrete state. σ_a and σ_b represent nonresonant background cross sections for transitions to continuum states that interact, respectively, do not interact with discrete autoionization states [20].

The data were analyzed by least-squares fit employing the program package MINUIT [21] that also supplies data handling as well as a double-convolution procedure for the theory routine. The recorded data $\sigma_s(E)$ are then given by

$$\sigma_s(E) = \int dE'' \int dE' \sigma(E') f(E'-E'';\Omega_M) g(E''-E;\Omega_D), \tag{2}$$

where $\sigma(E')$ is the photoionization spectrum, which is convoluted by the experimentally determined monochromator function f and a Doppler broadening function g. Here, Ω_M and Ω_D stand for monochromator resolution and Doppler broadening, respectively. The function $g(E''-E)$, which represents the Doppler broadening due to thermal motion of atoms, is a pure Gaussian function. The Doppler half width (Ω_D) is given by [22]

$$\Omega_D = 2h\nu\left(2\ln 2\frac{k_B T}{Mc^2}\right)^{1/2}, \tag{3}$$

with M being the mass of the atom, T the temperature of the gas, c the speed of light, and k_B the Boltzmann constant, respectively. For a photon energy of $h\nu=64.135$ eV and $T=300$ K, as realized in the present experiments, the Doppler broadening Ω_D amounts to 0.457 meV (FWHM) for ^{3}He and 0.396 meV (FWHM) for ^{4}He. The total experimental resolution Ω_T is approximately given by $(\Omega_M^2+\Omega_D^2)^{1/2}$.

In the simplest approximation, which is normally assumed in the data analysis, the monochromator resolution function f is simulated by a pure Gaussian function. In the present case, however, this was found to be insufficient in describing the experimental spectra. Deviations of the monochromator resolution function from a pure Gaussian have been reported before for high-resolution XUV monochromators [2,3]. Here we used two different approaches for simulating the monochromator resolution function. In the first monochromator-resolution model, $f(E'-E'';\Omega_M)$ is described by the sum of two Gaussians ($G+G$), in the second model, by a Gaussian plus a Lorentzian function ($G+L$):

$$f(E'-E'';\Omega_M) = \alpha G(E'-E'';\Omega_G) + (1-\alpha)H(E'-E'';\Omega_H), \tag{4}$$

where G stands for a Gaussian and H for a Gaussian or a Lorentzian function, respectively, Ω_G and Ω_H are the widths of the functions G and H, respectively, and α determines the weights of the two distributions contributing to the monochromator resolution function.

In the present work, we employed Eq. (2) for the fit analysis of resonances $2,-1_3$, $2,1_4$, and $2,0_7$ in ^{3}He and ^{4}He, with the two different models described above. To improve the reliability of the fit results, a parallel double-convolution fit

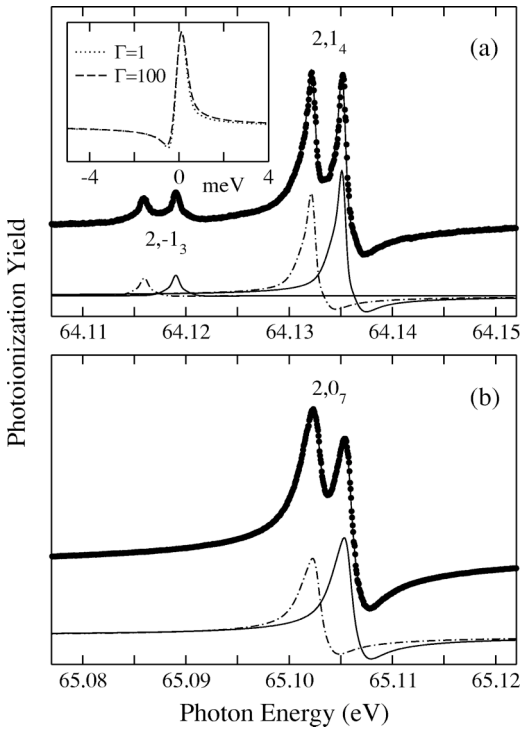

FIG. 2. Photoionization spectra of a ^{3}He-^{4}He gas mixture recorded in the regions of (a) the $2,-1_3$ and $2,1_4$ resonances; and (b) the $2,0_7$ resonance of doubly excited helium. The solid lines through the data points represent the fit results obtained with a monochromator function consisting of a Gaussian plus a Lorentzian (for details, see text). The solid (dash-dotted) subspectra represent the resonances of ^{4}He (^{3}He). Simulations of a resonance with $q=3$, and with $\Gamma=1$ and 100 μeV, respectively, are plotted in the inset of (a) using a Gaussian resolution function with a width of 1 meV.

procedure was applied, with three scans of the resonances $2,-1_3$ and $2,1_4$, and one scan of resonance $2,0_7$.

A numerical convolution of the $2,-1_3$ resonance spectra is very time-consuming due to the small value of Γ. Very recently, Lambourne *et al.* [18] have succeeded in measuring the natural width of the $2,-1_3$ resonance directly by following the fluorescence decay of the $2,-1_3$ resonance, with the result of $\Gamma=3.5\pm0.6$ μeV; this experimental result agrees very well with the theoretical value of $\Gamma_{th}=3.18$ μeV previously obtained by Liu *et al.* taking radiative and nonradiative decay processes into account [11]. In order to avoid numerical difficulties in the data analysis caused by the small natural width, we set $\Gamma=20$ μeV for the fit analysis of this resonance. This approach was justified by simulations where a Fano resonance with a given value of q and different values of $\Gamma(1,3,10,30,100$ μeV) was convoluted with a Gaussian function of 1 meV width. The simulated spectra were found to be practically identical, in particular for values of $\Gamma \leqslant 30$ μeV; the results of two simulations for $q=3$, and with $\Gamma=1$ μeV and $\Gamma=100$ μeV, respectively, are shown in the inset of Fig. 2(a).

Figure 2 presents the best fit results for the resonances $2,-1_3$, $2,1_4$, and $2,0_7$ of ^{3}He and ^{4}He, using the described double-convolution fit procedure (monochromator resolution and Doppler broadening). The displayed fit results were obtained with the monochromator resolution function given by the $(G+L)$ model, where the Gaussian function describes pre-dominantly the central peak, while the Lorentzian simulates the tails of the monochromator resolution function. Note that the lines of the resonances in ^{3}He seem to be broader than those in ^{4}He; this is actually not due to the increased Doppler broadening of the ^{3}He resonances, as one might expect, but is essentially caused by the superposition of two Fano resonances. A detailed comparison of the subspectra reveals only minor differences in the total widths. The obtained monochromator resolution function is displayed in Fig. 3, together with the one obtained by the $(G+G)$ model.

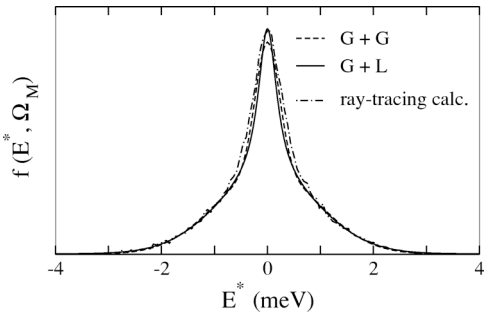

FIG. 3. Derived resolution function $f(E^*,\Omega_M)$ of the PGM monochromator, $E^*=E'-E''$ is the energy with respect to the monochromator energy E', G+G represents one monochromator-resolution model given by the sum of two Gaussians, while $G+L$ stands for the other model given by the sum of a Gaussian and a Lorentzian function. The dash-dotted curve represents the results of ray-tracing simulations (see text).

IV. RESULTS AND DISCUSSION

A. Fit results and resonance parameters

The obtained fit parameters derived from the two models $(G+G$ and $G+L)$ are summarized in Table I, which shows that the results depend only weakly on the specific fit model. For the resonance $2,1_4$, the results for q, Γ, E_r agree well with theoretical predictions. For the resonance 2, 0_7, the obtained values for q and Γ do not agree within the error bars with the theoretical results. In this case, saturation effects due to a relatively high pressure of $\cong$400 μbar in the gas-ionization cell cannot be excluded, and would actually explain the observed differences. The q value for the resonance $2,-1_3$ is slightly smaller than the theoretical value of -23.39, a difference that might originate from the fixed value assumed for Γ in the fit or from the influence of the radiative decay, which contributes substantially to the decay of this resonance [11]. These contributions were not taken into account in the calculations. The experimental energy positions E_r of all three resonances agree within the error bars with the theoretical values.

In addition to the simultaneous fits, all spectra were fitted individually using the monochromator resolution function obtained from the parallel fits. The error bars given in Table I were derived from the scattering of the fit parameters using

TABLE I. Resonance energies E_r, natural widths Γ, and Fano parameters q, obtained from double-convolution fits using two different models for the monochromator-resolution function G+G and G+L, respectively. For comparison, recent theoretical results from the literature are also given. The numbers in parentheses represent the error bars in units of the last digit.

		$2,-1_3$	$2,1_4$	$2,0_7$
Γ (μeV)	Theory[a]	3.18	60.13	610.56
	Theory[b]	0.28	55.20	649.01
	Experiment[c]	3.5(6)		
	$G+G$	[d]	56(13)	775(200)
	$G+L$	[d]	57(12)	833(55)
q	Theory[b]	−23.39	−3.32	−2.53
	$G+G$	−14.4(27)	−3.21(70)	−2.28(1)
	$G+L$	−16.5(40)	−2.96(70)	−2.28(1)
^{4}He E_r (eV)	Theory[b]	64.118	64.134	65.107
	G+G	64.119(2)	64.135(1)	65.106(1)
	$G+L$	64.119(2)	64.135(2)	65.106(1)
ΔE (meV)	$G+G$	3.05(17)	3.00(2)	3.10(5)
	$G+L$	3.04(15)	3.00(2)	3.10(6)

[a]Reference [11].
[b]Reference [23].
[c]Reference [8].
[d]Value fixed during fit; see text.

the different fit approaches. The best fits were obtained by simulating the monochromator resolution function by a Gaussian line shape plus a Lorentzian line shape (resulting in a reduced chi squared, $\chi_r^2=1.58$). The fits with two Gaussians for the monochromator resolution function were found to be slightly worse ($\chi_r^2=1.75$).

B. Isotope shifts

As can be seen from the obtained resonance energies, all resonances exhibit an isotope shift, i.e., the resonances in ^{3}He are shifted by 3.06 ± 0.07 meV to lower energies as compared to ^{4}He. This observation is in good agreement with theoretical expectations, when contributions from both the NMS and the SMS are considered.

The isotope shifts ΔE of the doubly excited resonances $2,-1_3$, $2,1_4$, $2,0_7$ caused by the NMS can be calculated using the well-known relation [24]

$$\Delta E = \frac{m_e}{m_p}\left(\frac{M_4 - M_3}{M_3 M_4}\right)E_{r,\infty}, \tag{5}$$

with m_e and m_p being the electron and the proton mass, respectively. M_3 (M_4) describes the mass of the nucleus in ^{3}He (^{4}He) in units of the proton mass and $E_{r,\infty}$ is the resonance energy in a hypothetical helium atom with infinite nuclear mass. Using the relation $E_{r,\infty}[1-(m_e/m_p)M_4] = E_{r,4}$ between $E_{r,\infty}$ and the resonance energies of ^{4}He, $E_{r,4}$, which can be derived from the experiment, we obtain $\Delta E=2.905$, 2.908, and 2.952 meV for the resonances $2,-1_3$, $2,1_4$, and $2,0_7$, respectively.

The shift in the energy of a resonance in ^{3}He and ^{4}He, caused by the specific mass shift (SMS), includes generally two contributions, one from the ground state and another one from the excited state. The SMS between the ground states of ^{3}He and ^{4}He results in a splitting of 198 μeV based on the calculations of Drake [25]. For the doubly excited states of helium, no theoretical results are available. However, Lindroth [26] has calculated the energy shift due to mass polarization for doubly excited states in the isoelectronic ion He^- below the $N=2$ ionization threshold resulting in value of $\cong$35 μeV. By assuming a similar situation for helium, we estimate the splitting between ^{3}He and ^{4}He caused by the SMS to be $\cong$10 μeV. This means that the contributions of the SMS between the doubly excited states of ^{3}He and ^{4}He are negligible in the present context.

The VS is caused by the monopole term of the Coulomb interaction between the electronic charge distribution in the atom and the protonic charge distribution within the nucleus. In good approximation, it is proportional to the difference of total electron densities at the nucleus between the two atomic levels involved $\Delta|\psi(0)|^2$, times the difference of the mean-squared nuclear charge radii of the two isotopes involved $\Delta\langle r^2\rangle$ [27]. As a consequence, the major contribution to the VS in the studied double-excitation resonances will originate from the ground state of helium, since the electron density at the nucleus in the double-excitation state N,K_n is expected to be about an order of magnitude smaller than that in the ground state. An exact value of the VS between ^{3}He and ^{4}He due to electric monopole interaction in the ground state ΔE_g^V is not available in the literature. Hence, we estimated ΔE_g^V by using the following equation from Ref. [27]:

$$\Delta E_g^V = |\psi(0)|^2 \frac{\pi a_0^3}{Z} C(\langle r^2\rangle, \Delta\langle r^2\rangle), \tag{6}$$

where $|\psi(0)|^2$ is the electronic charge density at the nucleus in the ground state of helium, with a_0 and Z representing the Bohr radius and the nuclear charge, respectively. C is the isotope-shift constant that depends on the mean-squared nuclear charge radius $\langle r^2\rangle$ and $\Delta\langle r^2\rangle$ [27]. On the basis of Eq. (6) and Ref. [28] [see Eq. (23) in this reference], we estimate ΔE_g^V to be of the order of a few 10 neV. To test the reliability of the described approximation, we also estimated the VS for the $1s2s(^3S)\rightarrow 1s2p(^3P)$ excitation in helium to be $\Delta E^V\cong 5$ neV, in good agreement with more detailed calculations that resulted in 3.49 neV [14]. In addition, Drake [29] evaluated the level shift in the ground state of ^{4}He caused by the finite protonic charge distribution in the nucleus to be $\delta E_g^V=124$ neV. Based on this value and the nuclear charge radii of ^{3}He and ^{4}He given by Shiner *et al.* [30], we estimate $\Delta E_g^V\cong 45$ neV, in good agreement with the above estimate based on Eq. (6). Since the nuclear charge radius of ^{3}He is larger than that of ^{4}He [r(^{3}He)=1.9506 fm, r(^{4}He)=1.673 fm [30]] the VS of the resonances between ^{3}He and ^{4}He have the same sign as the MS. Here, we took into account that the level shift due to electric monopole interaction in the doubly excited states of the helium atom

are much smaller that those in the ground state.

This leads to total isotope shifts of $\Delta E = 3.103$, 3.106, and 3.150 meV for the resonances $2,-1_3$, $2,1_4$, and $2,0_7$, respectively. These numbers are in good agreement with the present experimental value of 3.06 ± 0.07 meV, reflecting the fact that the NMS as well as the SMS of the ground-state energies of He are fully sufficient for understanding the experimental results. The largest effect is due to the NMS that contributes $\cong 96\%$ to the total isotope shift. All additional contributions, such as the SMS in the excited states or the VS, give only minor contributions; specifically, the contribution of the VS is negligible within the present experimental accuracy.

C. Monochromator resolution function

In Fig. 3, the derived monochromator resolution functions $f(E^*, \Omega_M)$ obtained from the two different models, are shown ($G+G$: dashed curve; $G+L$: solid curve). The shapes of the two resolution functions derived from the experimental data display only minor differences. Both consist of a narrow peak and broad shoulders at lower and higher energies, which clearly underline our finding that a single Gaussian is not always sufficient for describing the monochromator resolution function of a high-resolution monochromator beamline. We were also able to reproduce the shape of the monochromator resolution functions by ray-tracing calculations using the program package RAY [31] and taking the properties of undulator radiation and the detailed optical design of the plane-grating monochromator into account; the results of these simulations are also presented in Fig. 3 in the form of the dash-dotted curve. It turned out that the resolution function of the U125/1-PGM monochromator is dominated by the F_{120}-aberration term of the focusing mirror (astigmatic coma [32]), while slope errors of its surface play only a minor role. Aberrations were calculated by integrating the optical path variation over the optical surface, weighed by the intensity distribution. Whenever aberrations are found to be the dominant factor, the energy resolution can be controlled by variation of the intensity distribution on the surface. A straightforward way of controlling the footprint pattern on the focusing mirror M_3 makes use of the angular properties of the undulator radiation.

By optimizing the photon flux at a given photon energy, the undulator gap is set to a specific value, where the angle-integrated photon flux is maximum. The photon energy is then redshifted with respect to the energy of the on-axis undulator harmonic. When the undulator is operated under these conditions, the angular intensity distribution of the undulator is no longer Gaussian shaped, but displays a flat top or even a doughnut shape. Figure 4 displays the monochromatic intensity distributions on focusing mirror M_3 of this beamline as a function of position z for two undulator settings with the undulator parameter $K=2.19$ and $K=2.18$, respectively. For the definition of the undulator parameter, see, e.g., Ref. [32].

The mentioned aberration term can be understood within a simplified picture. Since the focal properties of the cylindrical focusing mirror M_3 are independent of the meridional coordinate, beams reflected on various parts of the mirror are focused at a fixed distance measured from the intercept point. Beams intercepting the focusing mirror in its center are focused onto the exit slit position, while others are focused before or behind the slit. In this way, the central beam gives rise to the sharp central maximum, whereas the defocused beams contribute to the broad base. The most significant effects of slope errors lead to a broadening of the sharp central peak.

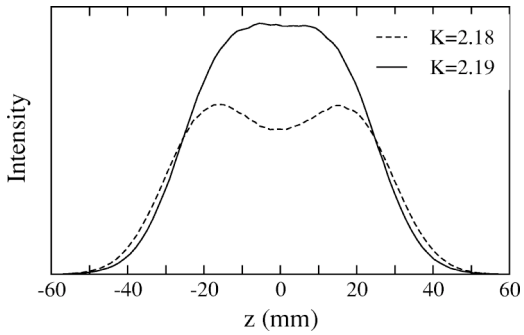

FIG. 4. Monochromatic intensity distribution on focusing mirror M_3 for the two undulator settings, with $K=2.19$ and 2.18, respectively.

If the monochromator is tuned to an even more redshifted photon energy, the angular distribution of the undulator results in a double-peaked illumination pattern at the focusing mirror. In this case, two pronounced beams (one left and one right) propagate downstream the beamline and form two foci close to the calculated exit-slit position. This can be understood on the basis of the specific optical design of beamline U125/1-PGM at BESSY II [33], shown in Fig. 5. The toroidal mirror M_1 and the plane mirror M_2 create an elliptical image of the circle on the position of the plane grating. Mirror M_1 also creates collimated light so that the c_{ff} value [$c_{ff}=\cos\beta/\cos\alpha$, with $\alpha(\beta)$ being the angle between the incoming (reflected) light and the surface normal of the grating] can be varied in order to obtain high flux or high resolution. During the measurements, a high c_{ff} value was used ($c_{ff}=12$) in order to achieve high resolution. As a consequence, the angle α between the surface normal of the grating and the incoming light was close to 90°, i.e., the grating was overfilled. The illumination pattern of the grating consists of two stripes perpendicular to the grooves of the grating, which means that these two rays illuminate different parts of the cylindrical focusing mirror M_3. Since this mirror focuses vertically on the exit slit, with a focal length of 10 m from the position where the light hits the mirror, the two different light rays impinging on the mirror will be focused vertically on two different positions on the axis of light propagation. During the experiments, the monochromator resolution was optimized by minimizing the total linewidth of the resonance $2,-1_3$. In this procedure, the position of the exit slit was varied and finally fixed at one of the two focal positions. The light focused on this position creates the narrow central part of the experimental resolution function, while the light focused either in front or behind this position causes the broad base.

In order to obtain a high spectral resolution without a broad base, one can use the blueshifted part of the undulator

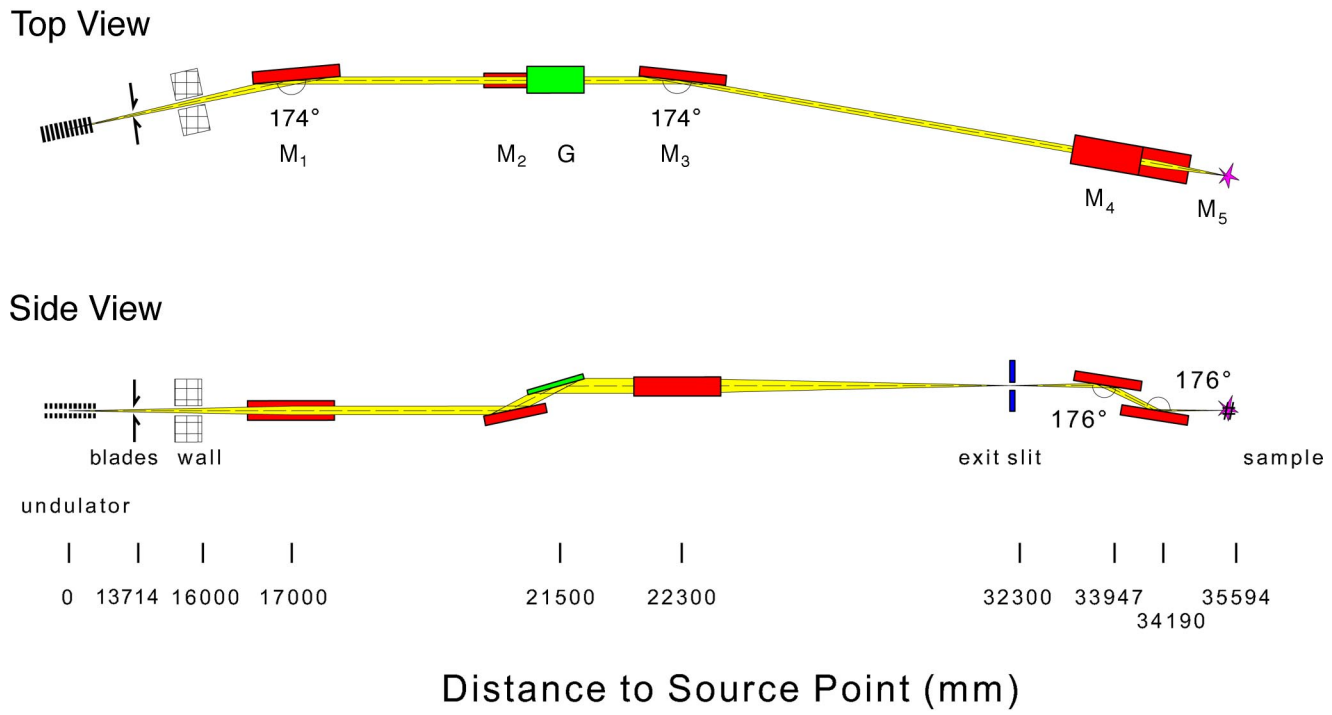

FIG. 5. Schematics of beamlime U125/1-PGM at BESSY II. Two plane gratings G with 300 and 1200 lines/mm can be selected. M_1: toroidal mirror with tangential radius $R=658760$ mm and sagittal radius $\rho=1772$ mm, M_2 plane mirror, M_3: cylindrical mirror with $\rho=1040$ mm, M_4: spherical mirror with $R=46200$ mm, M_5: cylindrical mirror with $\rho=101$ mm.

peak. In this case the light originates from the central part of the electron beam axis so that the entire light can be focused onto the exit slit. This, however, can only be achieved for the price of a weaker photon flux, since the intensity drops quite fast on the blue side of an harmonic undulator peak.

V. SUMMARY AND CONCLUSIONS

In the present work, the ^{3}He-^{4}He isotope shifts of the doubly excited resonance states $2-1_n$ ($n=3$ to 6), $2,1_n$ ($n=4$ to 7), and $2,0_7$ were determined by measuring photoionization spectra with high spectral resolution using synchrotron radiation. The experimentally derived isotope shift of 3.06 ± 0.07 meV was found to be in good agreement with theoretical estimates that vary from 3.103 to 3.150 meV for the different resonances studied, based on the NMS and the SMS; the VS was estimated to be negligibly small with respect to the present experimental accuracy. With a reliable double-convolution fit procedure that includes Doppler broadening, the resonance energies and Fano profiles of some of the resonances were analyzed, and good agreement between the derived parameters and the theoretical results was found. The resolution function of the monochromator was derived and compared with the results of ray-tracing calculations, taking into account the properties of undulator radiation as well as the specific design of the plane-grating monochromator beamline.

ACKNOWLEDGMENTS

This work was supported by the Bundesministerium für Bildung und Forschung, Project No. 05 KS1KED/0, and the Deutsche Forschnungsgemeinschaft, Project No. PU 180/1-1. Y.H.J. thanks the MPI für Physik Komplexer Systeme, Dresden, for financial support.

[1] R. P. Madden and K. Codling, Phys. Rev. Lett. **10**, 516 (1963).
[2] M. Domke, G. Remmers, and G. Kaindl, Phys. Rev. Lett. **69**, 1171 (1992).
[3] K. Schulz, G. Kaindl, M. Domke, J. D. Bozek, P. A. Heimann, A. S. Schlachter, and J. M. Rost, Phys. Rev. Lett. **77**, 3086 (1996).
[4] M. Domke, K. Schulz, G. Remmers, G. Kaindl, and D. Wintgen, Phys. Rev. A **53**, 1424 (1996).
[5] J.-E. Rubensson, C. Såthe, S. Cramm, B. Kessler, S. Stranges, R. Richter, M. Alagia, and M. Coreno, Phys. Rev. Lett. **83**, 947 (1999).
[6] M. K. Odling-Smee, E. Sokell, P. Hammond, and M. A. MacDonald, Phys. Rev. Lett. **84**, 2598 (2000).
[7] R. Püttner, B. Grémaud, D. Delande, M. Domke, M. Martins, A. S. Schlachter, and G. Kaindl, Phys. Rev. Lett. **86**, 3747 (2001).
[8] J. G. Lambourne, F. Penent, P. Lablanquie, R. I. Hall, M. Ahmad, M. Žitnik, K. Bučar, M. K. Odling-Smee, J. R. Harries, P.

Hammond, D. K. Waterhouse, S. Stranges, R. Richter, M. Alagia, M. Coreno, and M. Ferianis, Phys. Rev. Lett. **90**, 153004 (2003).
[9] T. W. Gorczyca, J. E. Rubensson, C. Såthe, M. Ström, M. Agåker, D. J. Ding, S. Stranges, R. Richter, and M. Alagia, Phys. Rev. Lett. **85**, 1202 (2000).
[10] J. M. Rost, K. Schulz, M. Domke, and G. Kaindl, J. Phys. B **30**, 4663 (1997).
[11] Ch.-N. Liu, M.-K. Chen, and C. D. Lin, Phys. Rev. A **64**, 010501(R) (2001).
[12] H. A. Bethe and E. E. Salpeter, *Quantum Mechanics of One- and Two-Electron Atoms* (Academic Press, New York, 1957).
[13] K. S. E. Eikema, W. Ubachs, W. Vassen, and W. Hogervorst, Phys. Rev. Lett. **76**, 1216 (1996).
[14] P. Zhao, J. R. Lawall, and F. M. Pipkin, Phys. Rev. Lett. **66**, 592 (1991).
[15] R. Follath, Nucl. Instrum. Methods Phys. Res. A **467-468**, 418 (2001).
[16] S. I. Fedoseenko, D. V. Vyalikh, I. E. Iossifov, R. Follath, S. A. Gorovikov, R. Püttner, J.-S. Schmidt, S. L. Moldtsov, V. K. Adamchuk, W. Gudat, and G. Kaindl, Nucl. Instrum. Methods Phys. Res. A **505**, 718 (2003).
[17] D. R. Herrick and O. Sinanoğlu, Phys. Rev. A **11**, 97 (1975).
[18] C. D. Lin, Phys. Rev. A **29**, 1019 (1984).
[19] U. Fano, Phys. Rev. **124**, 1866 (1961).
[20] U. Fano and J. W. Cooper, Phys. Rev. **137**, A1364 (1965).
[21] http://www.info.cern.ch/asdoc/minuit/
[22] See, e.g., W. Demtröder, *Laser Spectroscopy* (Springer, Berlin, 1988).
[23] B. Grémand and D. Delande (private communication).
[24] H. Kopfermann, *Nuclear Moments* (Academic Press, New York, 1958), p. 162.
[25] G. W. F. Drake, Nucl. Instrum. Methods Phys. Res. B **31**, 7 (1988).
[26] E. Lindroth, Phys. Rev. A **52**, 2737 (1995).
[27] See, e.g., A. Steudel, in *Hyperfine Interactions*, edited by A. J. Freeman and R. B. Frankel (Academic Press, New York, 1967).
[28] W. Humbach, Z. Phys. **133**, 589 (1952).
[29] G. W. F. Drake, in *Long-range Casimir Forces: Theory and Recent Experiments on Atomic Systems*, edited by F. S. Levis and D. A. Micha (Plenum Press, New York, 1993).
[30] D. Shiner, R. Dixson, and V. Vedantham, Phys. Rev. Lett. **74**, 3553 (1995).
[31] F. Schäfers, BESSY Techn. Bericht **202**, 1 (1996).
[32] W. Peatman, *Gratings, Mirrors and Slits, Beamline Design for Soft X-Ray Synchrotron Radiation Sources* (Gordon, Amsterdam, 1997).
[33] R. Follath, F. Senf, and W. Gudat, J. Synchrotron Radiat. **5**, 769 (1998).